Ranah Research
Journal of Multidisciplinary Research and Development
E-ISSN: 2655-0865
DINASTI RESEARCH
082170743613 ranahresearch@gmail.com https://jurnal.ranahresearch.com

DOI: https://doi.org/10.38035/rrj.v8i5

Prediction of Specific Capacitance and Equivalent Series Resistance of Activated Carbon-Based Supercapacitors Using an Adaptive Neuro-Fuzzy Inference System

Mulyati Mulyati[1], Galang Persada Nurani Hakim[2]
[1]Faculty of Engineering, Mercubuana University, Jakarta, Indonesia,
55424110004@student.mercubuana.ac.id
[2]Department of Informatics Engineering, Mercu Buana University, Jakarta, Indonesia,
galang.persada@mercubuana.ac.id

Corresponding Author: galang.persada@mercubuana.ac.id[2]

Abstract: *Supercapacitors are attracting growing interest as energy storage devices owing to their high power density and long cycle life. Their performance depends strongly on the electrode material, particularly activated carbon with its complex pore architecture. The relationship between characterization parameters and both specific capacitance (Cs) and equivalent series resistance (ESR) is non-linear and difficult to model conventionally. This study develops a predictive model based on an Adaptive Neuro-Fuzzy Inference System (ANFIS) using secondary data from forty samples reported in international scientific literature. Input variables comprise specific surface area (SBET), pore volume (Vp), pore diameter (Dp), crystallite size, diffraction angle, and surface functional groups, with the dataset partitioned at a ratio of 80:20 for training and testing. Evaluation demonstrates that ANFIS attains a coefficient of determination of 0.9851 for Cs and 0.9901 for ESR, surpassing Random Forest across every metric. ANFIS yields RMSE = 8.8 F/g and MAE = 4.5 F/g for Cs, and RMSE = 0.08 Ω and MAE = 0.04 Ω for ESR. Surface plot analysis reveals a synergistic interaction between SBET and Vp on Cs and the effect of crystal structure on ESR. The model captures complex relationships accurately while remaining interpretable through membership functions and fuzzy rules.*

Keywords: *activated carbon, supercapacitor, ANFIS, specific capacitance, equivalent series resistance*

INTRODUCTION

The need for reliable energy storage technology continues to grow as the use of portable electronic devices, electric vehicles, and renewable energy systems expands. Among the various options available, supercapacitors emerge as superior candidates due to their high power density, fast charge-discharge process, and cycle life far exceeding that of conventional batteries (Sasikumar et al., 2024). These characteristics make supercapacitors particularly relevant for applications that demand instant energy response as well as long-term reliability.

The performance of a supercapacitor is largely determined by the material properties of the electrode used (Cuéllar, 2024). Activated carbon is one of the most intensively studied materials, given its large specific surface area, complex pore architecture, and adequate chemical and mechanical resistance. The micro and nanostructures of activated carbon allow the storage of electrical charges either through the electric double layer (EDL) mechanism or pseudocapacitance arising from the functional groups on its surface (Boorboor Ajdari et al., 2020). A number of characterization parameters, including specific surface area (SBET), pore volume (Vp), pore diameter (Dp), pore size distribution, degree of crystallinity and graffiti, and type of surface function group, together affect the electrochemical performance of the material. Specific capacitance (Cs) as a key marker of charge storage capacity is strongly influenced by the size of the effective surface area and the ease with which electrolyte ions access the pore structure, while equivalent series resistance (ESR) describes the internal constraints of the system relating to material conductivity, interparticle connectivity, and ion movement efficiency (Sujiono et al., 2022).

The relationship between characterization parameters and electrochemical performance is complex and non-linear, so these parameters interact with each other simultaneously. Expansion of surface area does not automatically increase capacitance if the pore structure is less supportive of ion movement, while the dominance of micropores has the potential to inhibit ion mobility and actually increase ESR. Neither linear regression nor simple correlation approaches have been able to describe the real relationships in these complex systems, while determining Cs and ESR through CV, GCD, and EIS testing requires time, cost, and specialized instruments (Cuéllar, 2024).

ANFIS was chosen because it combines neural network learning capabilities with fuzzy inference, making it more effective in handling uncertainty and non-linear systems on limited data than deep learning (Chebaane et al., 2025). Theoretically, this research enriches the literature on the application of ANFIS to complex material systems, and practically offers an alternative to predicting electrochemical performance without relying entirely on expensive experimental testing (Zhu et al., 2021). The research was limited to secondary data from various journals with SBET, Vp, Dp, crystallinity, and functional group inputs, as well as Cs and ESR outputs. The novelty lies in the simultaneous modeling of Cs and ESR using heterogeneous datasets, different from previous studies which were generally homogeneous and focused on a single performance indicator (Imtiaz et al., 2024).

METHOD

Data Source and Preparation

The modelling process relied on secondary data compiled from peer-reviewed publications reporting the physicochemical characterization and electrochemical performance of activated carbon electrodes. After screening, unit harmonization, and removal of incomplete records, forty samples were retained as the working dataset. Each record contains six characterization descriptors, namely specific surface area (SBET), pore volume (Vp), pore diameter (Dp), crystallite size, diffraction angle (2θ), and surface functional groups, paired with two performance indicators, Cs and ESR. Because the descriptors differ substantially in magnitude and unit, every variable was normalized prior to training so that no single input dominated the learning process merely because of its numerical scale. Restricting the dataset to studies that report characterization and electrochemical testing within a single publication was intended to preserve internal consistency between the input descriptors and their corresponding output values (Pedro, 2023).

ANFIS Modeling

The ANFIS model is constructed with a configuration of six characterization parameters as *Input* and two models *Output* which are separate, namely Model 1 for Cs prediction and Model

2 for ESR prediction. Each model uses a *Fuzzy Inference System* (FIS) Sugeno with the amount *Membership function* (MF) as many as two pieces per variable *Input*, and trained over fifty epochs using a hybrid learning algorithm. Sugeno Architecture was chosen for producing *Output* in the form of linear functions that are easier to optimize computationally. Mathematically, the final output of the Sugeno-type ANFIS model can be expressed as the weighted sum of all the normalized fuzzy rules, namely:

$$y = \sum_{i=1}^{n} \bar{w}_i f_i \qquad (1)$$

The ANFIS architecture used in this study can be described through five sequential layers, namely the fuzzification layer, the fuzzy rule layer, the firing strength layer, the normalization layer, and the consequent–output layer.

Layer 1 – Fuzzification. Each numerical input is mapped into a fuzzy membership degree using the generalized bell membership function:

$$\mu_{A_{rj}}(x_j) = \frac{1}{1+\left|\frac{x_j - c_{rj}}{a_{rj}}\right|^{2b_{rj}}} \qquad (2)$$

where $\mu_{Arj}(x_j)$ is the membership degree of the j-th input in the r-th fuzzy rule, x_j is the j-th input variable, a_{rj} controls the width of the membership function, b_{rj} controls the shape or slope of the curve, and c_{rj} denotes the center of the membership function.

Layer 2 – Fuzzy Rules. Fuzzy rules are formed using the IF–THEN format:

$$R_r: \text{If } x_1 \text{ is } A_{r1}, x_2 \text{ is } A_{r2}, \dots, x_m \text{ is } A_{rm}, \text{then } f_r \qquad (3)$$

where R_r is the r-th fuzzy rule, A_{rj} is the fuzzy set for the j-th input, m is the number of input variables, and f_r is the consequent output of rule r.

Layer 3 – Firing Strength. The firing strength of rule r is obtained from the product of all input membership degrees:

$$w_r = \prod_{j=1}^{m} \mu_{A_{rj}}(x_j) \qquad (4)$$

If the number of membership functions per input is equal, the theoretical number of fuzzy rules is:

$$R = q^m \qquad (5)$$

where q is the number of membership functions per input and m is the number of input variables.

Layer 4 – Normalization. Each firing strength is normalized against the total firing strength of all rules:

$$\bar{w}_r = \frac{w_r}{\sum_{r=1}^{R} w_r} \qquad (6)$$

Layer 5 – Sugeno Consequent. In the first-order Sugeno inference system, the output of each rule is expressed as a linear function of the inputs:

$$f_r = p_{r0} + p_{r1}x_1 + p_{r2}x_2 + p_{r3}x_3 + p_{r4}x_4 + p_{r5}x_5 + p_{r6}x_6 \qquad (7)$$

where p_{r0}, p_{r1}, …, p_{r6} are consequent parameters obtained through the ANFIS training process.

Output Layer. The final ANFIS output is the weighted sum of all rule outputs based on the normalized firing strength:

$$\hat{y} = \sum_{r=1}^{R} \bar{w}_r f_r \qquad (8)$$

For the Cs prediction model, the final output is written as:

$$\widehat{C_s} = \sum_{r=1}^{R} \bar{w}_r f_r^{C_s} \qquad (9)$$

while for the ESR prediction model it is written as:

$$\widehat{ESR} = \sum_{r=1}^{R} \bar{w}_r \, f_r^{ESR} \qquad (10)$$

each with its own set of consequent parameters trained independently through the ANFIS learning process.

Partitioning was carried out through random permutation, allocating eighty percent of the records to the training subset and the remaining twenty percent to the testing subset. Randomization was applied to suppress sampling bias and to keep both subsets representative of the overall data distribution. Model parameters were adjusted by minimizing the discrepancy between predicted and observed values on the training subset, after which predictive capability was assessed on the testing subset, which had never been exposed to the model during learning.

Comparative Model

Random Forest was employed as a benchmark to position the performance of ANFIS against an established data-driven regression technique. The benchmark model was implemented in MATLAB as a bagged ensemble of regression trees and was trained on precisely the same training partition, the same six input descriptors, and the same normalization scheme as the ANFIS models, so that any difference in outcome could be attributed to the modelling approach rather than to differences in data handling. Random Forest was selected because it accommodates non-linear relationships and multivariable interactions without requiring an explicit functional form, yet it does not expose the reasoning behind its predictions in a form that can be inspected by the analyst (Xiong et al., 2019).

Evaluation Metrics Value

Quantitative evaluation was carried out using three statistical metrics. RMSE is calculated using the equation:

$$RMSE = \sqrt{\frac{1}{n} \sum_{i=1}^{n} (y_i - \hat{y}_i)^2} \qquad (11)$$

MAE is counted as:

$$MAE = \frac{1}{n} \sum_{i=1}^{n} | y_i - \hat{y}_i | \qquad (12)$$

While the determination coefficient is expressed as:

$$R^2 = 1 - \frac{\sum_{i=1}^{n} (y_i - \hat{y}_i)^2}{\sum_{i=1}^{n} (y_i - \bar{y})^2} \qquad (13)$$

RESULTS AND DISCUSSION

Results

Model Convergence

Training is monitored through an error curve against the epoch (Figure 1). Errors in both models decreased sharply at the beginning of training, then sloped to converge with no indication of overfitting. The Cs model shows a more stable convergence, reflecting a consistent parameter-capacitance relationship, while the ESR model shows greater initial fluctuations, indicating the complexity of the relationship between the material structure and internal resistance.

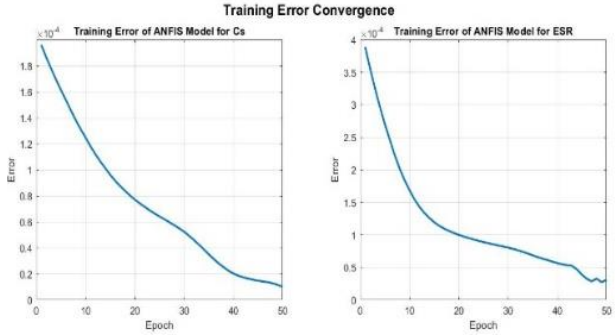

Figure 1. Training Error Convergence ANFIS model for Cs and ESR prediction

Membership Function

The membership function (MF) represents the input-output relationship in a fuzzy logic framework. Each input variable is modeled using the generalized bell function (gbellmf) which is divided into two categories, low and high (Figure 2). Smooth and overlapping curves show continuous interpolation capabilities so that predictions are not discrete.

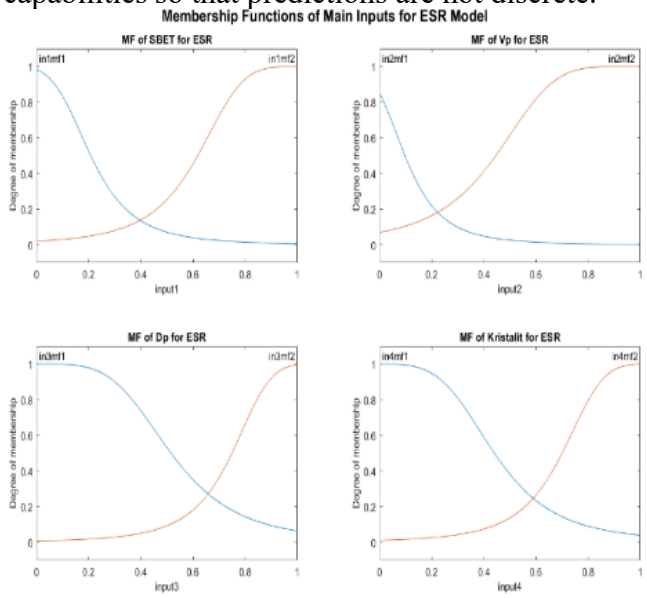

Figure 2. Membership function of the main input variable in the ANFIS model for ESR prediction

Evaluation of the ANFIS Model

Comparison of Actual and Predicted Values

Model evaluation was carried out using test data that was completely separate from the training data. Based on scatter *plot* analysis with an ideal reference line (y = x), most of the data points in both the Cs and ESR models are tightly scattered around the diagonal line, which indicates a high degree of correspondence between the actual and predicted values. In the Cs model, there are some points that deviate slightly from the ideal line, especially in the range of high capacitance values, but these deviations are still within acceptable tolerance limits. Meanwhile, the ESR model shows a tighter point distribution and closer to the ideal line, which indicates higher accuracy. The value of the determination coefficient obtained was $R^2 = 0.9851$ for Cs and $R^2 = 0.9901$ for ESR. These values show that the model is able to explain more than 98% of the data variation, which is a very high achievement in the context of data-driven modeling. Expressed in absolute terms, the capacitance model deviated from the observed values by 8.8 F/g in RMSE and 4.5 F/g in MAE, whereas the resistance model deviated by 0.08 Ω and 0.04 Ω respectively. Both magnitudes remain small relative to the operating range of each parameter, indicating that the residual variance is distributed evenly rather than concentrated in a particular segment of the data.

Performance Comparison between ANFIS and Random Forest

The two modelling approaches were evaluated on an identical testing partition using three statistical measures. The complete figures are presented in Table 1, while their relative magnitudes are visualized in Figure 3.

Table 1. Evaluation results of the ANFIS and Random Forest models

Output	Model	RMSE	MAE	R^2
Cs	ANFIS	8,8	4,5	0,9851
Cs	Random Forest	18,5	14,0	0,93
ESR	ANFIS	±0,08	±0,04	0,9901
ESR	Random Forest	±0,20	±0,15	0,92

ANFIS registered smaller prediction errors than Random Forest for both targets. On the capacitance model, the error was reduced by more than half in RMSE and by roughly two-thirds in MAE, while the coefficient of determination rose from 0.93 to 0.9851. A comparable pattern emerged on the resistance model, where RMSE and MAE fell to less than half of the benchmark values and the coefficient of determination increased from 0.92 to 0.9901. The consistency of this advantage across two physically distinct outputs suggests that the improvement does not stem from a favourable partition of one particular target, but from the capacity of the hybrid architecture to represent graded transitions between input states.

The gap becomes intelligible when the internal mechanics of both approaches are considered. Random Forest constructs its prediction from a collection of piecewise-constant partitions, so its response surface changes in discrete steps whenever a splitting threshold is crossed. Characterization descriptors such as pore diameter and crystallite size, however, influence electrochemical behaviour in a gradual manner rather than through abrupt thresholds. The generalized bell membership functions employed in ANFIS overlap continuously, allowing a sample to hold partial membership in more than one linguistic category simultaneously and thereby producing smoother interpolation across the descriptor space (Pedro, 2023).

Based on the results of the evaluation, the ANFIS model produced lower RMSE and MAE values than *Random Forest*, both for Cs and ESR. The R^2 value of ANFIS is also consistently higher. Visually, this is reflected in Figure 3, where the ANFIS bar is lower in RMSE and MAE, and higher in R^2.

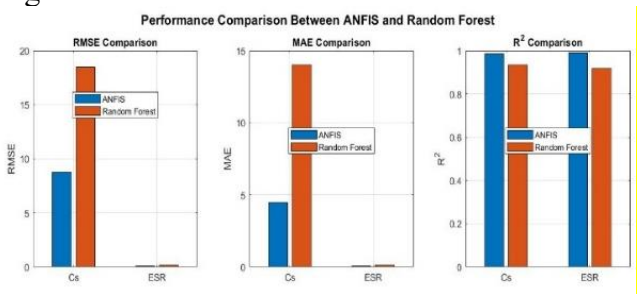

Figure 3. Comparison of the performance of the ANFIS and Random Forest models based on RMSE, MAE, and R^2 metrics

Surface Plot Analysis: Influence of S~BET~ and V~p~ on Cs

The analysis of the relationship between material parameters and supercapacitor performance was carried out through the visualization of *the surface plot* of the ANFIS model. Based on Figure 4, the value of Cs tends to increase as S~BET~ and V~p~ increase. A high S~BET~ condition accompanied by a high V~p~ results in a maximum Cs value, which indicates a synergistic effect.

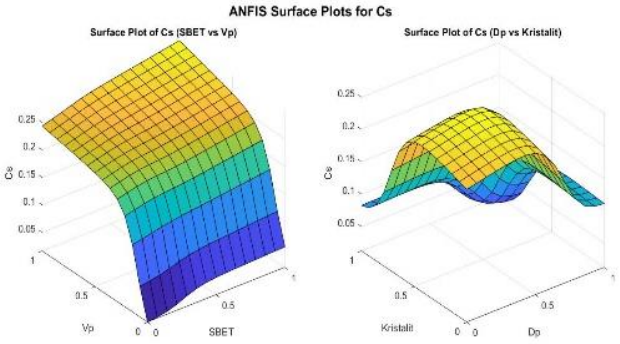

Figure 4. Surface plot of the relationship between S~BET~ and V~p~ to specific capacitance (Cs)

Theoretically, this phenomenon can be explained through the energy storage mechanism in *an electric double-layer capacitor* (EDLC). Capacitance depends on the active surface area of the electrode as per the equation $C = \varepsilon A/d$, where C is the capacitance, ε is the permittivity of the electrolyte, A is the active surface area, and d is the distance between charges. Materials with

high S~BET~ provide more active areas for the formation of electrical double layers, while large V~p~ supports more effective diffusion of electrolyte ions into the internal structure of the material.

Surface Plot Analysis: The Influence of Material Structure on ESR

Based on Figure 5, ESR values tend to decrease in materials with more optimal pore structure. ESR is affected by several factors, including electrode material resistance, contact resistance, electrolyte resistance, and ion diffusion resistance in the pore. In materials with good pore distribution, electrolyte ions can move more freely through the internal structure, so that diffusion resistance is reduced and ionic conductivity is increased.

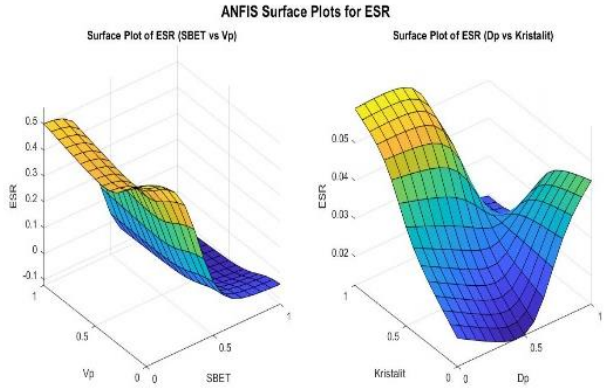

Figure 5. Surface plot relationship between material structure parameters and equivalent series resistance (ESR)

The surface plot shows that the combination of D~p~ and crystalite size has an influence on ESR. Pores that are too small inhibit the movement of ions, while pores that are too large reduce the area of the active surface. The more regular size of the crystalite also contributes to the increased electrical conductivity of the material, thus helping to lower internal resistance. These results show that the ESR value is a function of the complex interaction between multiple parameters, rather than the result of a single variable.

Discussion

Validation of the Literature

Supercapacitors are known to be able to balance high power density with adequate energy capacity, making them relevant for a wide range of modern energy storage applications (Supercapacitors et al., 2021). The Cs value predicted by the ANFIS model ranges from 100–420 F/g, consistent with reported values in the literature. For instance, activated carbon of kenaf fiber with a surface area of 3,359 m^2/g produced a capacitance of 312 F/g (Subramaniam et al., 2024), in line with model prediction trends in high-performance materials. However, the relationship of specific surface area to capacitance is not always linear (And, 2018), as ion access limitations and sub-optimal pore size distribution can reduce effectiveness even at high SBET values.

Effect of Pore Structure on Electrochemical Performance

The pore structure plays a central role in the electrochemical performance of activated carbon. Micropores provide a large surface area for charge storage, while mesopores act as ion transport pathways that accelerate diffusion (Jadhav & Glynn, 2025). The surface plot of this study shows a non-linear interaction between SBET and Vp against Cs, consistent with the ion transport mechanism where a good pore structure increases the diffusion coefficient and charge kinetics (Engineering, 2020). Pore diameters in the mesoporous range of 2–3 nm are considered

optimal, as the AC-K1 sample with a Dp of 2.1 nm showed the highest Cs, confirming this relevance in ANFIS modeling.

Effect of Crystallinity and Functional Clusters on ESR

The structure of the activated carbon crystal also determines the ESR through the electron conduction mechanism; Higher degrees of graphitization provide better conduction paths thus lowering internal resistance (Zahra et al., 2024). On the other hand, surface functional groups such as hydroxyl (–OH), carboxyl (–COOH), and carbonyl (C=O) increase pseudocapacitance through redox reactions, but if excessive increases resistance and decreases material stability (Tetra et al., 2018). The surface plot of the study's ESR is in line with the mechanism, where more regular crystallite parameters are associated with lower ESR values.

Advantages of ANFIS and Comparison with Other Approaches

In terms of interpretability, ANFIS has advantages over black-box approaches such as Random Forest and XGBoost. The combination of fuzzy logic and artificial neural networks allows ANFIS to model complex and non-linear input-output relationships in an adaptive manner (AbdElRhiem et al., 2025), is particularly relevant considering the relationship between the characterization parameters of activated carbon and electrochemical performance is multi-variable and nonlinear (Dong et al., 2025).

New Data Prediction and Material Design Implications

Predictions of new material data show that the AC-K1 sample (activated carbon of kenaf fiber, SBET 3,359 m^2/g, Vp 1.2 cm^3/g, Dp 2.1 nm) has optimal performance. Among the coconut shell samples, the AC1 with the highest SBET (1,234.5 m^2/g) showed the best performance, confirming the potential of local biomass as a cheap and environmentally friendly supercapacitor electrode, in line with studies reporting high capacitance in biomass-based activated carbon (Li et al., 2024), (Kocyigit et al., 2025). The ANFIS model is thus proven to serve as an initial material selection tool prior to experimental testing.

Taken together, the findings establish that the characterization descriptors of activated carbon govern supercapacitor performance through interacting rather than isolated pathways, and that a neuro-fuzzy architecture is able to reproduce these interactions while still exposing its reasoning through membership functions and interpretable rules. The novelty of this work rests on modelling capacitance and internal resistance simultaneously from a single heterogeneous dataset drawn from multiple laboratories, whereas earlier studies have generally relied on homogeneous data and confined themselves to one performance indicator. This dual-output formulation permits a candidate material to be screened for charge storage capacity and for internal resistance in one pass, positioning the model as a preliminary selection instrument that precedes rather than replaces experimental verification.

CONCLUSION AND SUGGESTIONS

Conclusion

This study succeeded in constructing an ANFIS-based predictive model for estimating the specific capacitance and equivalent series resistance of activated carbon in supercapacitor applications. Trained on forty secondary records with an 80:20 partition, the model reached a coefficient of determination of 0.9851 for Cs and 0.9901 for ESR, surpassing Random Forest on every evaluation metric. Prediction errors settled at RMSE = 8.8 F/g and MAE = 4.5 F/g for capacitance, and at RMSE = 0.08 Ω and MAE = 0.04 Ω for resistance. Surface plot analysis demonstrated that capacitance rises through the joint contribution of specific surface area and pore volume rather than through surface area alone, while resistance declines when pore geometry and crystallite regularity jointly favour ion transport and electron conduction. The

model therefore captures multivariable non-linear behaviour with accuracy while retaining interpretability through its membership functions and fuzzy rules.

Limitations

Several boundaries constrain the interpretation of these results. First, the dataset was assembled from published literature, so its coverage is bounded by what previous studies chose to report, and the forty records available restrict the breadth of material variation the model could learn. Second, the input space was confined to six characterization descriptors, whereas supercapacitor behaviour is also shaped by electrolyte type and concentration, current density, scan rate, operating voltage, electrode mass, and cell configuration, none of which entered the model. Third, secondary data inevitably carry heterogeneity in synthesis routes and testing protocols across the source laboratories. Fourth, validation was performed exclusively on a held-out subset of the same secondary data; no primary experimental measurement was conducted to verify the predictions under controlled laboratory conditions.

Suggestions

Subsequent work is encouraged to enlarge the dataset so that the model can learn a wider range of material characteristics, particularly at the upper end of the capacitance range and the lower end of the resistance range. Direct experimental data should be gathered as an independent validation set, since predictions verified against controlled measurement carry substantially greater confidence than those tested on secondary records alone. The input space warrants extension to electrochemical and testing variables, given that Cs and ESR respond to measurement conditions as well as to material structure. Further optimization of the ANFIS configuration is also advisable, covering the number and type of membership functions, the epoch count, the method of generating the initial fuzzy inference system, and the validation scheme. Comparison against additional intelligent methods such as artificial neural networks, support vector regression, or gradient boosting variants would clarify which approach best suits this modelling problem. Finally, the trained model could be embedded in a lightweight software tool so that practitioners are able to estimate electrode performance during preliminary material design.

Acknowledgment

Mulyati was responsible for conceptualization, literature curation, data collection and preparation, ANFIS model development, formal analysis, and preparation of the original draft. Galang Persada Nurani Hakim was responsible for methodological supervision, validation of the modelling procedure, interpretation of results, and critical review and editing of the manuscript. Both authors have read and approved the final version submitted for publication.

REFERENCES

AbdElRhiem, E., Abdelaziz, S. M., Barakat, Y. F., Mohamed, S. G., & Lebda, H. I. (2025). A theoretical and experimental study on indentation creep with x-silica addition to an Al–8Zn composite alloy, based on Adaptive Neuro-Fuzzy Inference System (ANFIS). *Materials Chemistry and Physics*, *341*, 130937. https://doi.org/https://doi.org/10.1016/j.matchemphys.2025.130937

And, M. J. R. (2018). Fabrication and Characterization of Activated Carbon from Charcoal Coconut Shell Minahasa, Indonesia. *Journal of Physics: Conference Series*.

Boorboor Ajdari, F., Kowsari, E., Niknam Shahrak, M., Ehsani, A., Kiaei, Z., Torkzaban, H., Ershadi, M., Kholghi Eshkalak, S., Haddadi-Asl, V., Chinnappan, A., & Ramakrishna, S. (2020). A review on the field patents and recent developments over the application of metal organic frameworks (MOFs) in supercapacitors. *Coordination Chemistry Reviews*, *422*, 213441. https://doi.org/https://doi.org/10.1016/j.ccr.2020.213441

Chebaane, S., Davoodabadi, S., Salem, T., Kolsi, L., Karimipour, A., & Aich, W. (2025). *Case*

Studies in Thermal Engineering ANFIS approach and thermal performance of solar air heaters integrated with phase change materials and porous foam gradient under mechanical vibrations. *72*(April).

Cuéllar. (2024). *Chemical synthesis and electrochemical performance of Hausmannite Mn3O4/rGO composites for supercapacitor applications*.

Dong, Y., Liu, Y., Mao, F., & Wu, H. (2025). Energy storage in supercapacitor researches: Interdisciplinary applications from molecular simulations to machine learning. *Applied Energy*, *393*, 126074. https://doi.org/https://doi.org/10.1016/j.apenergy.2025.126074

Engineering, C. (2020). *from coconut shell charcoals for supercapacitors Preparation of porous graphene-like material from coconut shell charcoals for supercapacitors*. *1916*. https://doi.org/10.1080/23311916.2020.1748962

Imtiaz, M., Alyousef, H. A., Alotaibi, B. M., Alrowaily, A. W., Alotiby, M. F., Farid, H. M. T., Al-Sehemi, A. G., & Hanaesh, A. M. A. (2024). Fabrication of cerium vanadate-embedded on carbon based graphene material (rGO) with significant performance for supercapacitor electrode. *Journal of Energy Storage*, *101*, 113987. https://doi.org/https://doi.org/10.1016/j.est.2024.113987

Jadhav, V., & Glynn, C. (2025). *Electrochemistry Communications Porous carbon nanotube electrodes in 3D printed symmetric supercapacitors with stable electrochemical response*. *177*(May). https://doi.org/10.1016/j.elecom.2025.107988

Kocyigit, N., Dinc, S., Yagci, O., & Busra, S. (2025). ZnO-NF / Graphene / Nafion as electrode platform for some pharmaceutical active ingredients sensor and energy storage applications. *Synthetic Metals*, *311*(June 2024), 117795. https://doi.org/10.1016/j.synthmet.2024.117795

Li, Y., He, G., Huang, Z., HuangFu, H., Li, Z., Qiao, Y., & Shi, Z. (2024). High-performance NF-loaded F-NiFe-LDH/rGO nanoflower/nanosheet composite electrode material achieving enhanced specific capacitance and energy density for supercapacitor. *Journal of Energy Storage*, *101*, 113954.

Pedro. (2023). Best practices for electrochemical characterization of supercapacitors. *Journal of Energy Chemistry*, *80*, 265–283.

Sasikumar, P., Karthikeyan, S., Arumugam, J., Devanesan, S., AlSalhi, M. S., Bencherif, H., & Krishnan, S. (2024). A facile one-step route to synthesize of novel porous reduced graphene oxide@nickel sulfide (rGO@Ni3S2) core shell nanostructures for high-performance supercapacitor electrodes. *Diamond and Related Materials*, *149*, 111614. https://doi.org/https://doi.org/10.1016/j.diamond.2024.111614

Subramaniam, T., Ansari, M. N. M., Krishnan, S. G., & Khalid, M. (2024). Kenaf-based activated carbon: A sustainable solution for high-performance aqueous symmetric supercapacitors. *Chemosphere*, *354*, 141593. https://doi.org/https://doi.org/10.1016/j.chemosphere.2024.141593

Sujiono, E. H., Zabrian, D., Zharvan, V., & Humairah, N. A. (2022). Results in Chemistry Fabrication and characterization of coconut shell activated carbon using variation chemical activation for wastewater treatment application. *Results in Chemistry*, *4*(November 2021), 100291. https://doi.org/10.1016/j.rechem.2022.100291

Supercapacitors, S., Lee, K., Shyan, M., Lim, W., Hong, Z., Chong, S., Tiong, T. J., Pan, G., & Huang, C. (2021). *Coconut Shell-Derived Activated Carbon for High-Performance*.

Tetra, O. N., Aziz, H., Syukri, S., Arifin, B., & Novia, A. (2018). Pengaruh Penambahan Karbon Aktif dari Tanah Gambut terhadap Kapasitansi Elektroda Superkapasitor Berbahan Dasar Karbon Aktif Cangkang Kelapa Sawit. *Jurnal Zarah*, *6*(2), 47–52.

Xiong, C., Li, B., Lin, X., Liu, H., Xu, Y., Mao, J., Duan, C., Li, T., & Ni, Y. (2019). The recent progress on three-dimensional porous graphene-based hybrid structure for supercapacitor. *Composites Part B: Engineering*, *165*, 10–46. https://doi.org/https://doi.org/10.1016/j.compositesb.2018.11.085

Zahra, T., Idris, A. M., Kumar, A., & Farid, H. M. T. (2024). Fabrication of high-performance of cost effective AgNbO3/rGO nanohybrid via hydrothermal route for supercapacitor applications. *Inorganic Chemistry Communications*, *170*, 113215. https://doi.org/https://doi.org/10.1016/j.inoche.2024.113215

Zhu, H., Zhu, L., Sun, Z., & Khan, A. (2021). Machine learning based simulation of an anti-cancer drug (busulfan) solubility in supercritical carbon dioxide: ANFIS model and experimental validation. *Journal of Molecular Liquids*, *338*, 116731. https://doi.org/https://doi.org/10.1016/j.molliq.2021.116731